Proposed Steady-State Kinetic Mechanism for *Corynebacterium ammoniagenes* FAD Synthetase Produced by *Escherichia coli*†

Igor Efimov,‡ Vladislav Kuusk,‡ Xiaoping Zhang,‡ and William S. McIntire*,‡,§

Molecular Biology Division, Department of Veterans Affairs Medical Center, San Francisco, California 94121, and Department of Biochemistry and Biophysics and Department of Anesthesia, University of California, San Francisco, California 94143

Received November 18, 1997; Revised Manuscript Received March 30, 1998

ABSTRACT: The bifunctional enzyme, FAD synthetase (FS), from *Corynebacterium ammoniagenes* was overproduced in *Escherichia coli* and purified, and its steady-state kinetic properties were investigated. Although FMN is an intermediate product in the conversion of riboflavin to FAD, FMN must be released after formation, and then rebind for adenylylation. It was shown that adenylylation of FMN is reversible; FAD and pyrophosphate can be converted to FMN and ATP by the enzyme. In contrast, under the conditions studied, phosphorylation of riboflavin is irreversible. A method is described for analysis of two catalytic cycles, occurring on one enzyme, which have a substrate and/or product in common. The binding order for the phosphorylation cycle of FS was established as riboflavin(in), ATP(in), ADP(out), and FMN(out). The order for the adenylylation cycle was ATP(in), FMN(in), pyrophosphate(out), and FAD(out). A set of steady-state constants was determined, and without additional optimization, these constants were sufficient to describe experimental progress curves for conversion of riboflavin to FAD. In independent studies, it was demonstrated that FMN binds to apo-FS with a dissociation constant of 6−7 μM, which is 2 orders of magnitude higher than the K_D value for riboflavin. For the steady-state kinetic analysis, this represents reversible binding of FMN(out) in the phosphorylation cycle (cycle I), which effectively inhibits catalysis in the adenylylation cycle (cycle II).

FAD synthetase (FS)[1] is a bifunctional enzyme, which catalyzes both phosphorylation of riboflavin (Rfl), producing FMN (ATP:riboflavin 5′-phosphotransferase, EC 2.7.1.26), and adenylylation of FMN, producing FAD (ATP:FMN adenylyltransferase, EC 2.7.7.2) (Scheme 1).

Manstein and Pai (*1*) reported that monomeric FS (M_r = 37 712 Da, as determined from the gene sequence) (*2*) catalyzes both phosphorylation and adenylylation, presumably at a single active site. It was also demonstrated that the activities depend on the presence of divalent cations, and some steady-state constants were provided for FS purified from *Corynebacterium ammoniagenes* (*1*).

Recently, the FS gene was cloned and overexpressed in *Escherichia coli* (*2*). Nakagawa et al. (*3*) studied the ability of the enzyme to produce FMN and FAD, primarily to find conditions for increasing the yields of these flavin forms. Although speculation was offered on how the enzyme functions on the basis of DNA sequence analysis and preliminary kinetic information that was presented (*2*), there has never been a detailed kinetic characterization of this small bifunctional enzyme. In this paper, we present a comprehensive steady-state kinetic mechanism, which includes both stages of the enzymatic conversion of Rfl to FAD.

MATERIALS AND METHODS

Materials. Materials and commercial sources were as follows: Tris Base (ultrapure), Boehringer Mannheim C; FAD (disodium salt), FMN (sodium salt), riboflavin, ATP (disodium salt), pyrophosphate (disodium, dihydrogen), ADP (sodium salt), disodium ethylenediaminetetraacectic acid (EDTA), and dithiotheritol (DTT), Sigma Chemical Corp.; $MgCl_2$, Alpha Chemical Corp.; and ATP determination kit (luciferase and luciferine), Molecular Probes, Inc.

Amplification of the FS Coding Sequence. *C. ammoniagenes* (ATCC6872) was cultured in LB medium at 30 °C. Genomic DNA was isolated from the cells as described by Silhavy et al. (*4*) and used as a template for amplification. The primer GGAATTCCATATGGATATTTGGTACGGAACAGCAGC and the reverse primer CGCGGATCCTTTTAGCTTTCTGCTTGTAGAAAG were synthesized on the basis of the published nucleotide sequence of FS (*2*). The forward primer corresponds to the N terminus of the protein, but the translation start codon GTG was replaced by ATG (underlined). The reverse primer corresponds to the C terminus. A DNA fragment of approximately 1 kb was amplified by the polymerase chain reaction (PCR). To confirm the accuracy of the amplification, the fragment was completely sequenced.

† This research was supported by a Department of Veterans Affairs Merit Review Grant, Program Project Grant HL-16251 from the National Heart, Lung and Blood Institute of the National Institutes of Health, an Academic Senate Grant, and a Research Evaluation and Allocation Committee Grant, University of California San Francisco.

* To whom correspondence should be directed: Molecular Biology Division (151-S), Department of Veterans Affairs Medical Center, 4150 Clement St., San Francisco, CA 94121. Telephone: (415) 387-1431. Fax: (415) 750-6959. E-mail: wsm@itsa.ucsf.edu.

‡ Department of Veterans Affairs Medical Center and Department of Biochemistry and Biophysics, University of California.

§ Department of Anesthesia, University of California.

[1] Abbreviations: DTT, dithiothreitol; FS, FAD synthetase (as pointed out by a referee, according to the Enzyme Commission on Nomenclature, the enzyme should rightfully be call a synthase, not a synthetase); HPLC, high-pressure liquid chromatography; PCR, polymerase chain reaction; Rfl, riboflavin.

S0006-2960(97)02817-1 CCC: $15.00
Published on Web 06/13/1998

Scheme 1

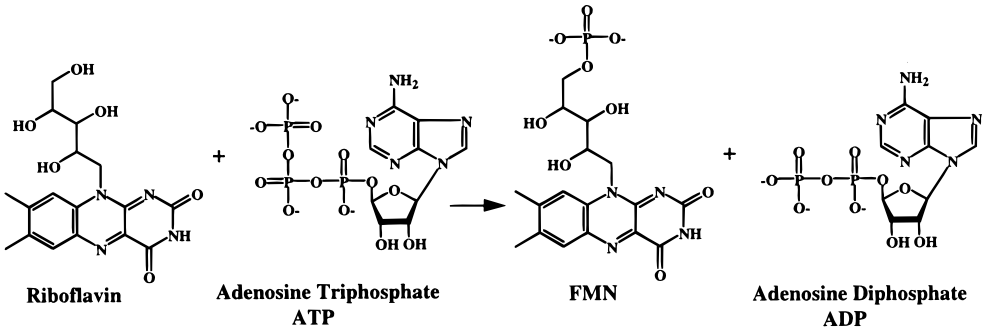

PHOSPHORYLATION REACTION

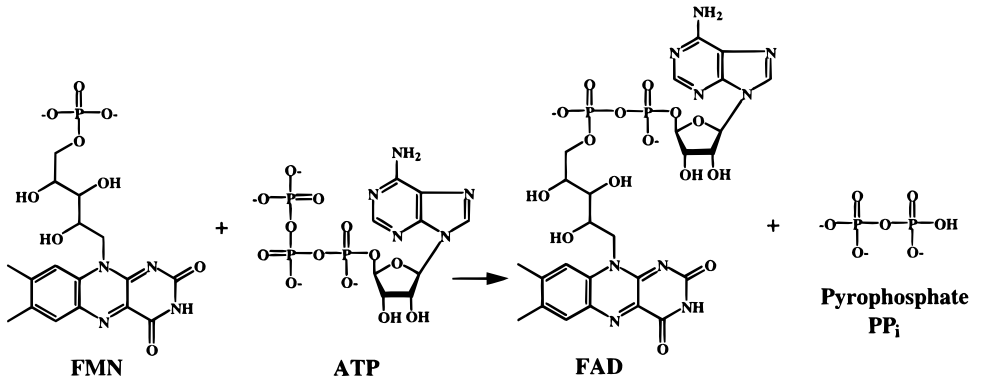

ADENYLYLATION REACTION

Production of FS by E. coli. A PCR-amplified fragment containing only the full-length coding region was digested with restriction enzymes *Nde*I and *Bam*HI. The resulting fragment was inserted into a *Nde*I−*Bam*HI site of pET-23a-(+), under control of the T7 promoter (Novagen). *E. coli* strain JM109(DE-3) was transformed with the recombinant plasmid, which contains a chromosomal copy of the gene for T7 RNA polymerase (Promega).

Purification of FS. Transformed *E. coli* cells were grown at 30 °C in 72 L of LB medium, which contained 200 mg/L ampicillin. After the cells were harvested with a Sharples centrifuge, the yield of cell paste was 260 g, and cells were stored at −20 °C. Cell paste (133 g) was suspended in 1 L of 100 mM Tris-HCl (pH 7.45) (unless otherwise noted, the pH of all Tris buffers was adjusted at room temperature, ∼21 °C, while all purification steps were performed at 4 °C), 10 mM EDTA, and 1 mM DTT. The suspension was cooled to 0 °C and twice passed through a two-stage Gaulin homogenizer (model 15-15MR-8TA) at 11 000 psi. The broken cells were centrifuged at 28000*g* for 45 min to yield 1.36 L of clarified solution. Solid $(NH_4)_2SO_4$ was added to 50% of saturation, and the resulting mixture was centrifuged at 28000*g*. The supernatant was then treated with solid $(NH_4)_2SO_4$ to 80% saturation, and after centrifugation, the pellet, containing the bulk of FS, was resuspended in 190 mL of 100 mM Tris-HCl, 1 mM EDTA, 1 mM DTT buffer (pH 7.45). The solution was dialyzed against 6 L of water for 1 h and then against 6 L of 50 mM Tris-HCl buffer for 2 h. The dialysis tubes were manually mixed every 15 min. After dialysis, the sample was diluted to 1 L with 50 mM Tris-HCl buffer and loaded onto a 21 cm (length) × 14 cm (diameter) DEAE-cellulose column. The column was washed with 2 L of 50 mM Tris-HCl buffer, and then with 3 L of 0.1 M NaCl in 50 mM Tris-HCl buffer. Enzyme was eluted with a 8 L gradient from 0.1 to 0.35 M NaCl in 50 mM Tris buffer. Activity was eluted from the column at about 0.2 M NaCl. As eluted, FS had a significant amount of FAD bound. This was determined by washing FAD from FS in Amicon Cetricon 10 centrifuge concentrators and recording the absorbance spectrum and fluorescence intensity of the filtrate. Thus, for use in preparation of FAD analogues, one needs first to rid the enzyme of FAD. It was also found that FS is not stable in low-ionic strength buffers (e.g., 10 mM Tris-HCl without salt).

FS was concentrated from 990 to 200 mL, in an Amicon ultrafiltration unit (YM-10 membrane). The sample was stored at −20 °C. Small portions of this sample were processed on a TSK 3000SW gel filtration column (7.5 mm × 300 mm) (Beckman/Altex). Final purification of the FS was done using Bio-Rad (Richmond, CA) CB-Q12 (quaternary amine anion exchange) resin packed in a Pharmacia HR10/10 column (1 cm × 10 cm), with a 0.1 to 0.3 M gradient of NaCl in 15 mM Tris-HCl buffer (pH 7.6) over a period of 40 min.

Activity Assays. Tris-HCl (50 mM, pH 7.6), 15 mM $MgCl_2$, 3 mM ATP, and 10 μM FMN were used for fluorescence (Hatachi F-4041 fluorescence spectrophotometer) measurements of activity during purification. Steady-state kinetic assays were carried out in 50 mM Tris-HCl buffer (pH 7.6, pH adjusted at 25 °C) and 10 mM $MgCl_2$ at 25 °C. The fluorescence intensities varied linearly with concentration at all levels of Rfl, FMN, and FAD (excitation λ = 446 nm and emission λ = 520 nm). Calibration of fluorescence was based on known extinction coefficients for

these flavins. The enzyme concentration was measured using an extinction coefficient ($\epsilon_{280} = 28\,500\ M^{-1}\ cm^{-1}$) calculated on the basis of the enzyme sequence (*5*).

FMN fluorescence titrations were conducted using the conditions described for the steady-state kinetic assays, with 3.2 and 6.7 μM FS. Titrations were preformed by adding FMN to solutions of the enzyme. The measurements were corrected for nonspecific quenching.

Progress Curves from High-Pressure Liquid Chromatography (HPLC) Analysis. Reaction mixtures were incubated at 25 °C. Aliquots were taken at various time for injection directly into the HPLC column. The flavin products were analyzed using a Beckman System Gold HPLC apparatus. Monitoring was done with a Gilson Spectra/glo Filter Fluorometer detector (excitation filter, 330−380 nm; emission filter, 430−600 nm). A Prodigy 5μ ODS(3) 100A, 100 mm × 4.6 mm column (Phenomenex) was used with a flow rate of 1.5 mL/min. The eluting solution was 10% acetonitrile in 50 mM potassium phosphate (pH 6.0).

Kinetic Data Treatment. Steady-state kinetic analyses and product and substrate inhibition studies were carried out like those outlined by Cornish-Bowden (*6*). The abbreviations follow those recommended by the International Union of Biochemistry and Molecular Biology (*7*). Numerical simulations were carried out using MATLAB, version 4.2c.1 (The MathWorks Inc., Natick, MA). Nonlinear fits were obtained using the NONLIN Shareware program (P. H. Sherrod, 4410 Gerald Pl., Nashville, TN).

RESULTS AND DISCUSSION

Production of C. ammoniagenes FS in E. coli. The PCR-amplified FS gene coding sequence was cloned into vector pET-23a(+). This recombinant plasmid was used to transform *E. coli* JM109(DE-3) cells, and the cells were cultured in Luria-Bertani broth (LB medium) at 28−30 °C. In contrast to cells containing the unmodified pET-23a(+) vector, the cell pellet containing the recombinant plasmid was yellow. Even in the absence of IPTG induction, the yield of FAD synthetase is about 30% of the total cytoplasmic protein. All of the FS was found in the soluble cell extract.

Steady-State Kinetic Studies. Although there are published experimental data concerning the effect of divalent cations on FS activity, it was decided that all assays would be carried out in the presence of saturating Mg^{2+} concentrations (=10 mM) to simplify the kinetic model. This leaves unanswered questions concerning the true role of a divalent cation and the existence and nature of a cation binding site in FS.

The investigation of the steady-state kinetic mechanism was divided into three separate parts, and then a hypothetical, comprehensive mechanism was checked for consistency by comparing rate and equilibrium constants obtained from these three parts. The parts are separate steady-state kinetic analysis of (i) the flavokinase (5′-phosphorylation of Rfl; cycle I), (ii) adenylyltransferase (adenylylation of FMN; cycle II) reactions, and (iii) progress curves of the reaction starting from Rfl, going to FAD, through an FMN intermediate. It should be noted that the FMN and ATP (product−substrate) link between the phosphorylation and adenylylation reactions places limitations on a complete kinetic analysis for each of these processes as isolated cycles, and since the analysis of the steady-state kinetic data for FS is somewhat complex and nontraditional, the chronological flow for the analysis is provided below.

Scheme 2

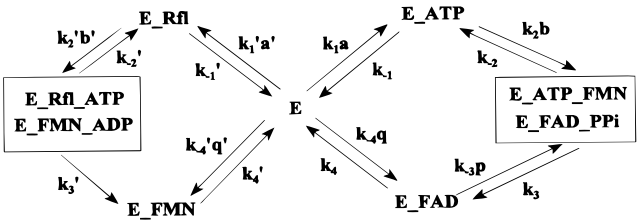

Step 1. The mechanisms for cycles I and II were established as compulsory ordered-binding mechanisms with an intermediate ternary complex.

Step 2. A scheme was constructed (Scheme 2), and equations for d[Rfl]/d*t* and d[FMN]/d*t* were derived. These equations contained terms that determined how each cycle is influenced by the other.

Step 3. Inhibition of the adenylylation reaction by FMN eliminated two possible binding orders for each of the cycles.

Step 4. The remaining binding orders for cycle II unambiguously described the influence of cycle II on cycle I. This allowed a choice between the remaining binding orders for cycle I.

Step 5. The established binding order in cycle I allowed us to choose the correct binding order for cycle II.

Step 6. With the binding orders established for both cycles, the values of the steady-state parameters were obtained by fitting eqs 2 and 4 (all equations and derivations are in the Appendix) to the experimental points by nonlinear regression.

Adenylylation of the FMN. From a preliminary HPLC analysis, it was found that the FAD → FMN reverse reaction takes place in the presence of Mg^{2+} and pyrophosphate. To check that this is truly a reversible reaction, the stoichiometric formation of ATP from FAD and pyrophosphate was established by a luciferin and luciferase chemiluminescence assay. It was found that the formation of ATP from FAD and pyrophosphate does not occur in the absence of Mg^{2+}, and there is no ATP formation in the absence of pyrophosphate. Under identical conditions, the ratio of rates for forward and reverse reactions remains the same (~0.7) in all fractions under the FS peaks from TSK and CBQ columns (see Materials and Methods). It was concluded that this is not a contaminating activity, and FS alone catalyzes the reaction in both directions.

The binding of FMN to apo-FS was investigated by a flavin fluorescence-quenching titration of the enzyme (see Materials and Methods for details). The experiment provides a K_D value for FMN of 7 ± 2 μM.

The adenylyltransferase activity of FS was studied by fluorescence assays, since the quantum yield of FAD fluorescence in aqueous solution is 12% of that of FMN. In steady-state kinetic experiments, at a single ATP concentration, substrate inhibition by FMN was observed (Figure 1). The ensuing steady-state kinetic analysis was carried out with lowered FMN concentrations, to avoid substrate inhibition by FMN. The initial steady-state kinetic analysis of the FMN adenylylation reaction eliminated a ping-pong type mechanism. Initial rates for forward and reverse reactions are

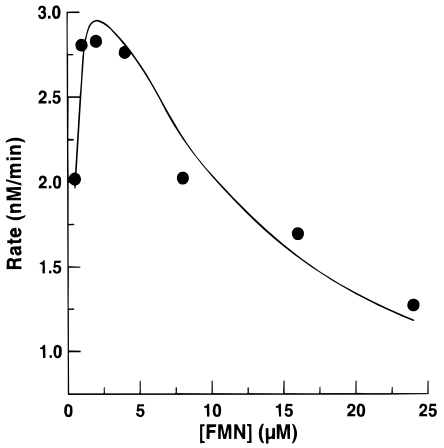

FIGURE 1: Substrate inhibition of the adenylylation cycle (cycle II) by FMN. The enzyme concentration was 5 nM. [ATP] = 12.5 μM, and [$MgC1_2$] = 10 mM, in 50 mM Tris-HCl at pH 7.6 and 25 °C. Note that substrate inhibition results from the influence of cycle I.

shown in panels A and B of Figure 2. Inhibition by products is shown in panels C−F of Figure 2. These data imply that this catalytic cycle (cycle II) operates by a compulsory ordered-binding mechanism. The effect of cycle I on this analysis will be discussed later.

Phosphorylation of Rfl. For initial rate studies, there is no change in fluorescence for the Rfl phosphorylation reaction, since Rfl and FMN have the same quantum yield. Therefore, the phosphorylation cycle (cycle I) was studied with a less convenient, and less accurate, HPLC technique so that [Rfl] and [FMN] could be monitored as a function of time.

Figure 3 shows the steady-state kinetic data for the reaction ATP + Rfl → ADP + FMN. The fact that the lines in Figure 3A are not parallel implies that this reaction also proceeds through a ternary complex. The reverse reaction, ADP + FMN → Rfl + ATP, could not be established definitively, even by increasing [E] 15-fold and [ADP] by as much as 200-fold (up to 1 mM, when 5−100 μM ATP is typical). Although some reaction occurs under these conditions, the increase in [Rfl] was camouflaged by its contamination in FMN, and the presence of ATP in the ADP preparation.

Establishing the Binding Order for Both Reaction Cycles. So far, it has been established that both the phosphorylation and the adenylylation cycles obey compulsory-ordered mechanisms. Additionally, it is known that the adenylylation step is reversible, but the phosphorylation is not. For the complete reaction from Rfl to FAD, FMN accumulates in the reaction mixture at concentrations much higher than that of FS, and there is substrate inhibition of the adenylylation cycle by FMN. These observations provide guidance for constructing a comprehensive steady-state kinetic mechanism.

A complete scheme was considered to be composed of two ordered-binding catalytic cycles, with only one enzyme form in common, namely, free FS. We propose the mechanism shown in Scheme 2. Although the final binding order is shown in the scheme, all possible binding orders were considered during the analysis.

In the following discourse, all primed terms will correspond to the first cycle (cycle I) and not primed to the second (cycle II). All abbreviations are in a standard form as described in the Appendix.

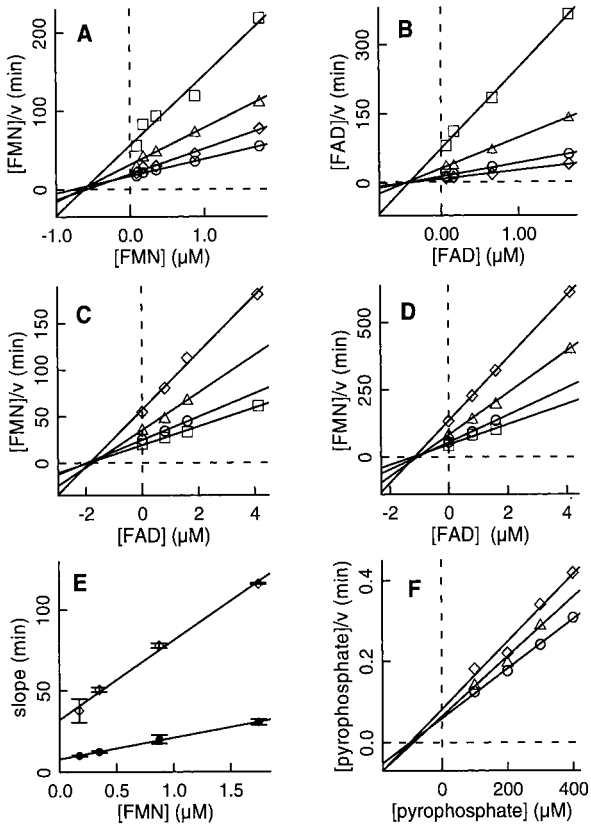

FIGURE 2: Plots of steady-state kinetic data for the FS adenylylation cycle (cycle II). The enzyme concentration was 4.5 nM, and [$MgCl_2$] = 10 mM. The units for the initial rates are micromolar per minute. (A) Initial rates (in the absence of products) for FMN to FAD conversion: (□) 5.9, (△) 14.8, (◇) 29.5, and (○) 59 μM ATP. (B) Initial rates for FAD to FMN conversion (in the absence of products): (□) 10, (△) 30, (○) 100, and (◇) 300 μM pyrophosphate. (C and D) Initial rates of FMN to FAD conversion in the presence of FAD. (C) [ATP] = 59 μM, and (D) [ATP] = 14 μM: (◇) 1.75, (△) 0.875, (○) 0.35, and (□) 0.175 μM FMN. (E) Slopes from plots C and D, as a function of [FMN]: (◇) 14 and (●) 59 μM ATP. Also displayed are error bars for each point. (F) Initial rates of FMN to FAD conversion in the presence of pyrophosphate where [ATP] = 45 μM: (◇) 0.575, (△) 0.144, and (○) 0.086 μM FMN.

Before the binding orders for each cycle were determined, it was deemed necessary to examine how one cycle affects the steady-state kinetic behavior of the other cycle. To aid in this endeavor, rate equations for changes in [Rfl] and [FMN] were derived (see the Appendix). Although the exact equations for each cycle contain terms from the other cycle, the binding order can be established solely from the patterns of product inhibition. All possible binding orders for each cycle are provided in Table 1.

Using the rate equation for FMN (eq 3), the existence of substrate inhibition observed in the steady-state kinetic experiments (Figure 1) indicates that FMN must be Q′ in cycle I and B in cycle II. This leaves as choices binding orders 1 and 4 for cycle I and orders 1 and 2 for cycle II (Table 1).

To determine the binding order in cycle I, the X_D term (see eq 5) must be defined. This term was unambiguously defined, after it was established that A is ATP and B is FMN in adenylylation cycle II (binding orders 1 and 2 in Table

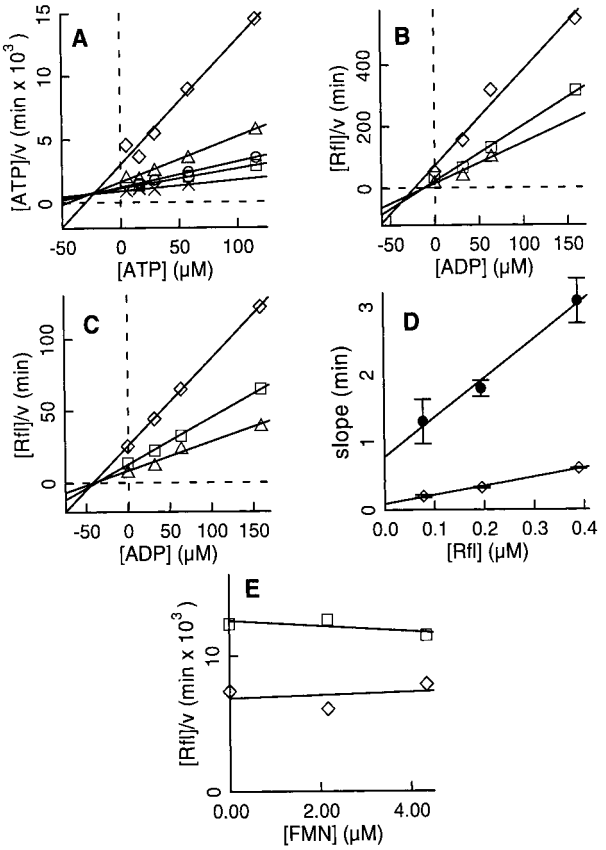

FIGURE 3: Plots of steady-state kinetic data for the phosphorylation cycle. In all assays, the enzyme concentration was 4.5 nM and $[MgCl_2] = 10$ mM. The units for the initial rates are micromolar per minute. (A) Initial rates of Rfl to FMN conversion in the absence of products: (◇) 44 nM, (△) 80 nM, (○) 160 nM, (□) 0.4 μM, and (×) 0.8 μM Rfl. (B and C) Initial rates of Rfl to FMN conversion in the presence of ADP. (B) [ATP] = 13 μM, and (C) [ATP] = 62 μM: (◇) 0.39 μM, (□) 0.19 μM, and (△) 78 nM Rfl. (D) Slopes from plots B and C as a function of [Rfl]: (●) 13 and (◇) 62 μM ATP. Also displayed are error bars for each point. (E) Initial rates of Rfl to FMN conversion in the presence of FMN where [ATP] = 6.1 μM: (□) 0.39 and (◇) 0.155 μM Rfl.

Table 1: Definitions of X'_D from Cycle I and X_D from Cycle II for Different Orders of Substrate Binding and/or Product Release

	binding order for cycle I				
	A′	B′	P′	Q′	X'_D
1	Rfl	ATP	ADP	FMN	q'/K'_{iQ}
2	ATP	Rfl	FMN	ADP	a'/K'_{iA}
3	Rfl	ATP	FMN	ADP	0
4	ATP	Rfl	ADP	FMN	$a'/K'_{iA} + q'/K'_{iQ}$

	binding order for cycle II				
	A	B	P	Q	X_D
1	ATP	FMN	PP_i	FAD	$(a/K_{iA})(1 + b/K_{mB})/(1 + K_{mA}b/K_{iA}K_{mB})$
2	ATP	FMN	FAD	PP_i	as above
3	FMN	ATP	PP_i	FAD	as above
4	FMN	ATP	FAD	PP_i	as above

1). With this information, it was possible to establish the correct order for cycle I.

This was accomplished by constructing plots of [Rfl]/v versus [ADP] at different Rfl and ATP concentrations (primary plots) and plots of primary slopes versus [Rfl] (secondary plots). These plots are shown in Figure 3. $\sum'$ in eq 6 contains terms with the product [ADP][Rfl], and the coefficient for this product defines the slopes in the secondary plot in Figure 3D (see the Appendix). The coefficient is a function of [ATP] for cases 1 and 3, but not cases 2 and 4, and since the slopes in secondary plots of Figure 3D are different for different ATP concentrations, binding order 4 is eliminated. Thus, the binding order was established for the phosphorylation cycle as Rfl(in), ATP(in), ADP(out), and FMN(out).

Table 2: Steady-State Kinetic Constants for FS[a]

K'_{iA}(Rfl)	0.079 ± 0.013 μM
K'_{mA}(Rfl)	very small (meaning $k'_3 \ll k'_1$ and $k'_3 \ll k'_4$)
K'_{iB}(ATP)	indeterminate
K'_{mB}(ATP)	89 ± 29 μM
K'_{iP}(ADP)	∞
K'_{mP}(ADP)	21.2 ± 2.4 μM
K'_{iQ}(FMN)[b]	5.8 ± 0.7 μM ($K_D = 7 \pm 2$ μM)
K'_{mQ}(FMN)	12 ± 1 μM
k'_{cat+}(Rfl → FMN)	0.41 ± 0.09 s^{-1}
k'_{cat-}(FMN → Rfl)	indeterminate
K_{iA}(ATP)	21.6 ± 4.0 μM
K_{mA}(ATP)	37.0 ± 7.2 μM
K_{iB}(FMN)	not determined
K_{mB}(FMN)	1.00 ± 0.15 μM
K_{iP}(pyrophosphate)	~60 μM
K_{mP}(pyrophosphate)	114 ± 25 μM
K_{iQ}(FAD)	0.64 ± 0.03 μM
K_{mQ}(FAD)	0.4 ± 0.1 μM
k_{cat+}(FMN → FAD)	0.300 ± 0.023 s^{-1}
k_{cat-}(FAD → FMN)	0.270 ± 0.023 s^{-1}

[a] All k_{cat} values were calculated from V/[E], where [E] = 4.5 nM. [b] $K_D = K'_{iQ}$. The K_D value, in parentheses, was determined by a FMN fluorescence quenching titration.

To finalize the analysis of cycle II, the order of product release needed to be determined. The influence of cycle I is provided in the equation $X'_D = [FMN]/K'_{iQ}$, and from linearized forms of the rate equation (eq 7), it follows that product Q should be a competitive inhibitor for case 1 and a mixed inhibitor for case 2. That is, the slopes of the lines in Figure 2E (the coefficient for the [FMN][FAD] term in eq 7) should be proportional to 1/[ATP] for case 1 but have very weak or no dependence on [ATP] for case 2. As seen in Figure 2E, the data are consistent with only case 1. It was determined that FAD is the last product to be released, and the order for the adenylylation step is ATP(in), FMN-(in), PPi(out), and FAD(out).

At this juncture, with the binding orders established for both cycles, additional experiments were carried out to facilitate the determination of more kinetic parameters. To obtain values of steady-state parameters, eqs 2 and 4 were fit to the experimental data by nonlinear regression. The resulting steady-state kinetic constants are shown in Table 2. With these parameters, the data in Figure 1, and eq 4, it was possible to determine the value of inhibition constant K'_{iQ} as 5.8 ± 0.7 μM, which is identical to the value of K_D determined from the FMN fluorescence-quenching titration (see Table 2). With the value of K'_{iQ}, analysis of the slopes in Figure 3D allowed for an estimation of the value of K'_{mQ} (=12 μM, Table 2).

To check the appropriateness of the entire proposed Scheme 2, progress curves were constructed for the reaction starting from Rfl, using an HPLC assay. Because FAD has low fluorescence, its concentration could be not measured at initial time points. Equations 2 and 4 describe the kinetics

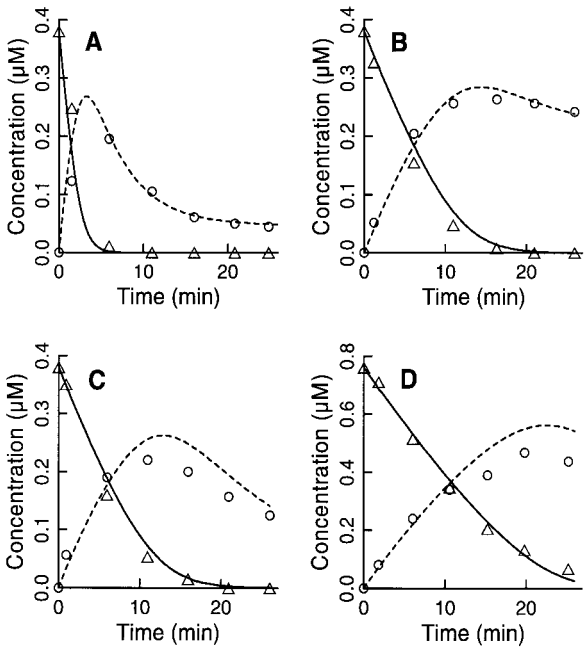

FIGURE 4: Progress curves measured by HPLC at various ATP and pyrophosphate concentrations: (△) [Rfl] and (○) [FMN]. Solid and dashed lines represent Rfl and FMN concentrations, respectively, calculated by simultaneously solving eqs 1 and 2 using the constants from Table 2. Initial concentrations were 18 nM FS for all curves; (A) 0.38 μM Rfl, 100 μM ATP, and 50 μM pyrophosphate; (B) 0.38 μM Rfl, 10 μM ATP, and 50 μM pyrophosphate; (C) 0.38 μM Rfl and 10 μM ATP; and (D) 0.78 μM Rfl and 10 μM ATP.

for the steady-state approximation. Stationary concentrations of various forms of enzyme are attained at an estimated time τ which was approximately 10 s. Thus, when $t \gg \tau$, a quasi-steady-state assumption was invoked, and these equations were used to describe progress curves for Rfl conversion to FAD, through FMN. Numerical simulations were performed by simultaneously solving the differential equations (eqs 2 and 4). The constants in these equations were not optimized, but the values of constants obtained from steady-state experiments for both cycles (Table 2) were used for the simulation. The comparisons of simulated and experimental data are displayed Figure 4. In the experimental substrate concentration intervals ([Rfl] = 0.38 and 0.76 μM, and [ATP] = 10 and 100 μM), and in the absence or presence of 50 μM pyrophosphate, theoretical curves are consistent with the experimental points. Interestingly, the progress curves in the presence of pyrophosphate are more consistent with simulated curves, although we believe that the all fits are quite good considering steady-state parameters and constants were used without adjustment. Thus, we feel these simulations support the proposed mechanism and justify the method of extracting of constants from initial rates measurements.

Closing Remarks. It is quite interesting, if not surprising, that FMN produced by FS in cycle I must be released to be involved in the second transformation to FAD. This phenomenon has a clear physiological purpose. Since *C. ammoniagenes* likely has FMN binding proteins, release of FMN after the first stage will provide the requisite FMN for these proteins.

Also very interesting are the findings that FMN binds after ATP in cycle II but Rfl binds before ATP in cycle I. The FMN fluorescence-quenching titration of apo-FS, and the FMN steady-state kinetic inhibition studies (Figure 1), provide conclusive evidence that FMN binding to apo-FS is equivalent to the reverse binding of FMN in cycle I (i.e., the reassociation of the final product released in this cycle; the k'_{-4}[FMN] step in Scheme 2), and this phenomenon disallows binding of ATP in a fashion that leads to FAD formation in cycle II. These observations lead to speculation about some aspects of the molecular mechanisms of action of FS. It seems that Rfl binding to FS allows ATP to bind in such a manner that the former is phosphorylated. On the other hand, when ATP binds first, FS is primed for adenylylation of FMN. [It is unknown whether Rfl can bind when ATP is bound in this "adenylylation site"; however, if Rfl does bind, perhaps no reaction would occur, because, presumably, the orientation and/or proximity would not be appropriate for phosphorylation (see Figure 5).] The fact that Rfl binds extremely tightly ($K'_{iA} = k'_{-1}/k'_1 = K_d = 79$ nM), but FMN binds to free FS 2 orders of magnitude less tightly (5.8 μM), is quite remarkable. It might be that there is an unfavorable (electrostatic?) interaction for FMN at the flavin binding site of free FS, but prior ATP binding ($K_{iA} = k_{-1}/k_1 = K_d = 21.6$ μM) suppresses this prohibition.

The adenylylation reaction is dependent on Mg^{2+} and does not occur in its absence. On the other hand, the phosphorylation reaction still occurs in the absence of Mg^{2+}, albeit less efficiently (*1*). A possible mechanism for adenylylation is one where β,γ-Mg^{2+}−ATP binds to free FS. The Mg^{2+} may complex with the phosphate group of incoming FMN and/or interact with a negative charge on the enzyme, which may be close to the (riboflavin-5′) phosphate binding site. Such an interaction could ease an unfavorable electrostatic interaction. A cartoon of the active site region(s) of FS is depicted in Figure 5. This hypothetical model shows a single binding site for the isoalloxazine and/or ribityl portions of the flavins, but two ATP sites, to accommodate the supposition that ATP binds differently in cycles I and II. A previous analysis of the deduced protein sequence has also implicated two ATP binding sites (*2*).

From an evolutionary point of view, incorporating the active sites for two reactions into one small protein is very efficient and effective. In mammals (e.g., rat liver), FMN and FAD formations are catalyzed by two different enzymes. Whereas *C. ammoniagenes* FS has a M_r of 38 000 Da (*2*), rat liver FMN synthetase (flavokinase, EC 2.7.1.26) has a M_r of 28 000 Da (*8*), and rat liver α_2 FAD synthetase (FMN → FAD, EC 2.7.7.2) has a M_r of 97 000 Da (*9*). Interestingly, the steady-state kinetic mechanism for each cycle of FS is very similar to that of the two enzymes from rat liver, in that each corresponding reaction has the same binding order. Beyond the mechanistic similarities, it will be interesting to see if there are any structural similarities between bacterial FS and the rat liver enzymes.

APPENDIX

The derivation of kinetic equations for the mechanism presented in Scheme 2 uses the following conventions. Primed terms are reserved for cycle I and have the same form as unprimed terms (except for X_N and X_D, which are defined below). All other abbreviations are in a standard form; capital letters designate species, and small letters concentrations. V_+ is the maximum rate for the forward

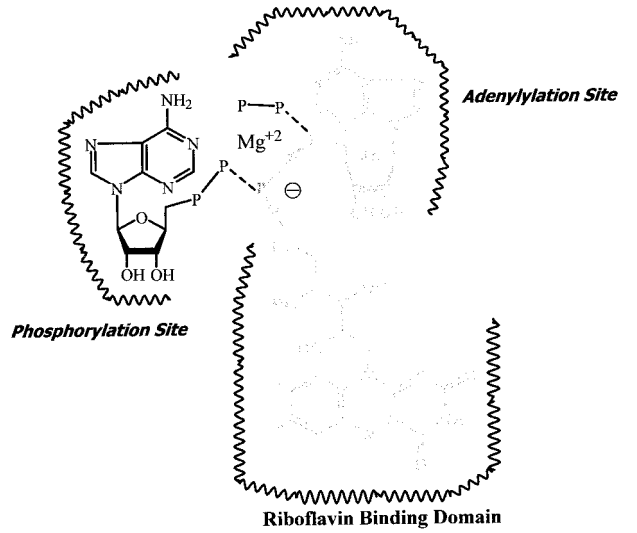

FIGURE 5: Highly idealized, hypothetical model for the active site of FS. The model attempts to accommodate all observations pertaining to the steady-state kinetic mechanism of this enzyme. There are two ATP binding sites, one where ATP binds for phosphorylation of Rfl and one where ATP binds for adenylylation of FMN. A single flavin binding site is proposed, where the isoalloxazine−ribityl moieties prefers to bind. In gray are the components of the final product, FAD. In cycle I, the solid gray arrow depicts the bond that is formed between the 5′-hydroxyl group of Rfl and the ATP γ-phosphate at the ATP phosphorylation Site. The black dashed line of this ATP represents the bond cleaved during this reaction. In cycle II, the gray dashed arrow represents the bond formed between the FMN 5′-phosphate and the α-phosphate of ATP at the ATP adenylylation site. The black dashed line is the bond cleaved as a result of this reaction. Also shown is a hypothetical negative charge near the FMN 5′-phosphate interaction site. Electrostatic repulsion between this charge and the phosphate would prevent FMN binding to free FS (note that there would be no such deterrent to binding of neutral Rfl). On binding of Mg^{2+}−ATP, placement of Mg^{2+} near this site could reduce the unfavorable electrostatic interaction and allow for FMN binding. Alternatively, binding of ATP to the adenylylation site causes a conformational change or movement of the FS negative charge [due to electrostatic interaction between this charge and ATP phosphate(s)], thus allowing FMN to bind.

reaction, and V_- is the maximum rate for the reverse reaction. The binding order is A(in), B(in), P(out), and Q(out). The task at hand was to devise methods that would establish the orders of substrate binding, and the order of product release for each cycle.

The standard equation for a two-substrate ordered-binding mechanism (isolated cycle) is

$$v = \frac{\frac{V_+ ab}{K_{iA}K_{mB}} - \frac{V_- pq}{K_{mP}K_{iQ}}}{\sum} \tag{1}$$

where

$$\sum = 1 + \frac{a}{K_{iA}} + \frac{K_{mA}b}{K_{iA}K_{mB}} + \frac{K_{mQ}p}{K_{mP}K_{iQ}} + \frac{q}{K_{iQ}} + \frac{ab}{K_{iA}K_{mB}} + \frac{K_{mQ}ap}{K_{iA}K_{mP}K_{iQ}} + \frac{K_{mA}bq}{K_{iA}K_{mB}K_{iQ}} + \frac{pq}{K_{mP}K_{iQ}} + \frac{abp}{K_{iA}K_{mB}K_{iP}} + \frac{bpq}{K_{iB}K_{mP}K_{iQ}}$$

To derive the steady-state rate equation for FMN, we used the King−Altman method, with the Goldstein−Volkenstein modifications (*6*). The derivation took into consideration the fact that the two cycles have free FS in common and that FMN, a product for cycle I, is also a substrate in cycle II. Note that the rate equation (eq 2), describing the time-dependent change in [FMN], has the same form independent of assigning FMN as A or B in cycle II, and as P′ or Q′ in cycle I.

$$\frac{d[FMN]}{dt} = \frac{-\frac{\Psi}{\Delta} + \frac{\Psi'}{\Delta'}}{\sum\frac{}{\Delta} + \sum'\frac{}{\Delta'} - 1} \tag{2}$$

where

$$\Psi = \frac{V_+ ab}{K_{iA}K_{mB}} - \frac{V_- pq}{K_{mP}K_{iQ}} \text{ and } \Delta = 1 + \frac{K_{mA}b}{K_{iA}K_{mB}} + \frac{K_{mQ}p}{K_{mP}K_{iQ}}$$

If each cycle had nothing in common with the other, then all terms for the other cycle disappear, and the equation reduces to a form which characterizes a one-cycle ordered-binding process (i.e., $a' = b' = p' = q' = 0$ in eq 2).

To investigate the influence of the binding order in cycle I on the rate equation for FMN, eq 2 is rewritten as

$$\frac{d[FMN]}{dt} = \frac{-\Psi + X'_N}{\sum + X'_D\Delta} \tag{3}$$

In the absence of Rfl and ADP, X'_N is zero, regardless of the binding order in cycle I. In contrast, X'_D will depend on binding order in cycle I as shown in Table 1. It should be noted that, if FMN were Q′ in cycle I and B in cycle II, then eq 3 would include a term that is functionally identical to rate of substrate inhibition by FMN. The equation for the rate of Rfl depletion is obtained in an analogous fashion.

$$\frac{d[Rfl]}{dt} = \frac{-\frac{\Psi'}{\Delta'}}{\sum\frac{}{\Delta} + \sum'\frac{}{\Delta'} - 1} = \frac{-\frac{\Psi'}{\Delta'}}{\sum'\frac{}{\Delta'} + X_D} \tag{4}$$

where

$$X_D = \frac{a}{K_{iA}} \frac{1 + \frac{b}{K_{mB}}}{1 + \frac{K_{mA}b}{K_{iA}K_{mB}}} \tag{5}$$

X_D is independent of the P and Q assignments in cycle II and has the same form regardless of the identity of A and B in this cycle.

To analyze the binding order in cycle I, we used the linearized form of eq 4:

$$-\frac{b'}{v'} = \frac{K'_{iA}K'_{mB}}{V'_+}\left[\sum'\frac{}{a'} + \frac{X_D}{a'}\left(1 + \frac{K'_{mA}b'}{K'_{iA}K'_{mB}} + \frac{K'_{mQ}p'}{K'_{mP}K'_{iQ}}\right)\right] \tag{6}$$

By first plotting [Rfl]/v versus [ADP] and then plotting slopes

from these curves versus [Rfl] for different ATP concentrations (secondary plots), we were able to determine whether the coefficient for the [Rfl][ADP] term is dependent on [ATP]. When Q′ ≡ FMN for cycle I, and A ≡ ATP for cycle II, then in the absence of FMN, $X_D = [ATP]/K_{iA}$. Thus, the slope in the secondary plot for case 1 in Table 1 is proportional to

$$\frac{1}{K'_{iA}K'_{mB}K'_{iP}} + \frac{1}{[ATP]}\frac{K'_{mQ}}{K'_{iA}K'_{mP}K'_{iQ}}$$

For case 4 in the table, it is proportional to

$$\frac{1}{K'_{iA}K'_{mB}K'_{iP}}$$

Thus, from the [ATP] dependence for the slopes of the secondary plots, it is possible to distinguish between binding orders 1 and 4.

To analyze the binding order for cycle II, when the binding order for cycle I is defined as Rfl(in), ATP(in), ADP(out), and FMN(out), the standard rules for analysis of the product inhibition patterns had to be modified, to take into account the influence of X'_D in eq 3, which, for this binding order, is defined as $[FMN]/K'_{iQ}$. The linearized form of eq 3 is

$$\frac{b}{v} = \frac{K_{iA}K_{mB}}{V_+}\left[\frac{\sum}{a} + \frac{X'_D}{a}\left(1 + \frac{K_{mA}b}{K_{iA}K_{mB}} + \frac{K_{mQ}p}{K_{mP}K_{iQ}}\right)\right] \quad (7)$$

When plotting [FMN]/v versus [FAD] at different FMN and ATP concentrations, and then plotting slopes from these plots versus [FMN] (secondary plots) at each [ATP], we were able to distinguish between orders 1 and 2 in Table 1. For case 1, the slope of secondary plots is proportional to

$$\frac{1}{[ATP]}\frac{K_{mA}}{K_{iA}K_{mB}K_{iQ}}$$

but for case 2, the slope will be proportional to

$$\frac{1}{K_{iA}K_{mB}K_{iP}} + \frac{1}{[ATP]}\frac{K_{mQ}}{K_{mP}K'_{iQ}K_{iQ}}$$

In the latter equation, the dependence on [ATP] is due to the influence from cycle I, and this dependence is very weak because of the large value of K'_{iQ} compared to K_{mQ} and is not balanced by the presence of K'_{mQ}, as was the case for cycle I.

REFERENCES

1. Manstein, D. J., and Pai, E. F. (1986) *J. Biol. Chem. 261*, 16169−16173.
2. Nakagawa, S., Hagihara, T., Fujio, T., and Aisaka, K. (1995) *Appl. Microbiol. Biotechnol. 43*, 325−329.
3. Nakagawa, S., Igarashi, A., Ohta, T., Hagigara, T., Fujio, T., and Aisaka, K. (1995) *Biosci., Biotechnol., Biochem. 59*, 694−702.
4. Silhavy, T. J., Berman, M. L., and Enquist, L. W. (1984) *Experiments with Gene Fusion*, Cold Spring Harbor Laboratory Press, Cold Spring Harbor, NY.
5. Pace, C. N., Vajdos, F., Fee, L., Grimsley, G., and Gray, T. (1995) *Protein Sci. 4*, 2411−2423.
6. Cornish-Bowden, A. (1995) *Fundamentals of Enzyme Kinetics*, Portland Press Ltd., London.
7. International Union of Biochemistry and Molecular Biology (IUBMB) (1992) *Biochemical Nomenclature and Related Documents* (Liébecq, C., Ed.) William Clowes and Sons, Ltd., London.
8. Merrill, A. H., and McCormick, D. B. (1980) *J. Biol. Chem. 255*, 1335−1338.
9. Oka, M., and McCormick, D. B. (1987) *J. Biol. Chem. 262*, 7418−7422.

BI972817J